https://doi.org/10.48048/tis.2022.6182

Experimental Examination on Finishing Characteristics of Aluminum Pipes in Magnetic Abrasive Machining Using SiC Contained Glued Magnetic Abrasives

Palwinder Singh[*] and Lakhvir Singh

Mechanical Engineering Department, Baba Banda Singh Bahadur Engineering College, Fatehgarh Sahib, Punjab 140407, India

([*]Corresponding author's e-mail: palwindergill13@gmail.com)

Received: 22 July 2021, Revised: 24 September 2021, Accepted: 30 September 2021

Abstract

With the rapid development in the industry, applications of finished parts are increasing day by day. However, the surface finish of the parts fabricated by conventional processes could not readily meet the requirements of various applications. Therefore, post-processing is needed to further improve the surface quality. Magnetic abrasive machining uses a flexible magnetic abrasive brush to remove material from the workpiece surface at a controllable rate. This cutting tool sticks to the workpiece during finishing operation and exerts a small force on the surface. In magnetic abrasive machining, the cutting tool neither requires compensation nor dressing. In this paper, the internal finishing of aluminum pipes has been investigated in magnetic abrasive machining tests using silicon carbide-based glued magnetic abrasives. For evaluating the performance of these magnetic abrasives, experimental work according to the central composite design technique was carried out to finish the aluminum pipes. The results so obtained were analyzed to study the influence of process parameters like magnetic field strength, speed of workpiece, abrasive mesh size and quantity of magnetic abrasives on percentage improvement in surface finish and material removal rate. The analysis showed that magnetic field strength was the most effective parameter while finishing the aluminum pipe followed by the quantity of magnetic abrasives. The finishing at optimal condition resulted in a surface finish of 0.07 μm. Further, scanning electron microscopy of the surface before and after magnetic abrasive machining was taken to study the improvement in surface finish.

Keywords: Magnetic abrasive machining, Finishing of pipe, Glued magnetic abrasives, Central composite design, Surface finish, Scanning electron microscopy

Introduction

With modernization and development in industries, there is a high demand for the surface finish in various industrial applications like medical, rocket, and aerospace parts, dies, semiconductor plants, etc. A process of inner magnetic abrasive machining (MAM) was proposed to produce the inner surface of the work specimen of the order of high finish. The non-traditional MAM process is an advanced method of machining that has the ability to remove microchips, in order to get surfaces of the highest surface finish. This process has been used to produce a microrelief layer. The specialty of the MAM process was the capability to control the flexibility of the tool. With ferromagnetic powder sealing by the magnetic field, one can control the density and rigidity of the flexible magnetic abrasive brush (FMAB), which helps to change the topography of magnetic flux in the working gap. Due to the small controllable cutting force, a damage-free surface can be produced after finishing the workpiece. This specialty of the MAM process differs from other finishing methods. MAM is an effective process, gives a good economic and ecological environment [1,2]. This method can finish different surfaces like the cylindrical, flat, bolt and complex shapes of ferromagnetic and non-magnetic materials. In practice, postprocessing is generally required to improve the surface finish of the manufactured parts for specific applications. Magnetic abrasive machining (MAM) is a nonconventional finishing method that could be employed to finish the confined area due to its flexibility [1]. Magnetic abrasive machining was initiated in the United States (US) in the 1930s where its first patent was produced in the 1940s with a remarkable growth era in the USSR and Bulgaria, Germany and Poland while the US in the 1960s continues the practical usage [2]. In the 1980s the Japanese started to conduct the research with various applications till in the 1990s, where MAM appeared with multifunctional practicals in the US as a machining process [3].

The growth of practical usage of materials manufacturing by MAM process such the semiconductor, aerospace materials and medical devices from optics industries have caused the continued development of enhanced methods for attaining a high form of surface finish accuracy and surface integrity [3].

Singh *et al.* [4]; Singh and Singh [5]; Singh and Singh [6] investigated the internal finishing of brass tubes with Al_2O_3 based sintered magnetic abrasives by MAM. The effect of several parameters on surface finish and material removal was studied. Patil *et al.* [7] proposed a method namely mechanically alloying to produce the magnetic abrasives to finish stainless steel SUS 304 tubes in MAM. They concluded that the best value of percentage improvement in surface finish (PISF*)* was obtained at a certain set of conditions. Kang *et al.* [8] finished bent tubes of SUS 304 stainless steel with diamond-based sintered magnetic abrasives by MAM. They concluded that surface finish was significantly influenced by machining time, percentage of diamond abrasives and speed. Kaushik *et al.* [9] worked on aluminum pipes using unbonded magnetic abrasives containing silica sand in MAM. They reported that the highest PISF was obtained as 73.15 %. Grewal *et al.* [10] prepared Al_2O_3 based sintered magnetic abrasives to finish brass pipes by MAM. They obtained the highest value of PISF of 50 % and the minimum surface roughness value of 0.16 µm. Jiao *et al.* [11] employed MAM for finishing the surface of the seal ring groove using Al_2O_3 based magnetic abrasives. It was found that the surface roughness from the initial Ra 4.3 µm decreased to Ra 0.6 µm. Sihag *et al.* [12] designed and fabricated chemo ultrasonic assisted magnetic abrasive finishing (CUMAF) set up. They reported that the CUMAF process resulted in a maximum PISF of 86.30 % was achieved at optimal processing conditions and pulse on time of ultrasonic vibrations among the 5 process variables had the maximum effect (21.99 %) on PISF. Yamaguchi *et al.* [13] employed MAM and magnetic field-assisted burnishing to post-process the SLM-ed SS316L disk. They reported that surface roughness was improved from 100 to 0.1 µm and compressive residual stress was imparted after MAM. However, this work did not consider the effects of various surface features or textures due to the changing normal direction of complex AM-ed parts which may not coincide with the laser-scanning plane of the layer-by-layer fabrication. Verma *et al.* [14] proposed a novel tool based on the MAM principle for finishing very small size holes and vertical surfaces. The stainless steel (SS304) pipe was finished and it was reported that a very fine surface finish of 0.56 nm was achieved. Deepak and Bhusan [15] experimentally analyzed the improvement in the surface finish of aluminum tubes by MAM. They reported that PISF increased with the increased value of current. It was further concluded that PISF increases up to the optimum value of grit size of abrasives and circumferential speed. Zhang *et al.* [16] polished selective laser melting manufactured (SLM-ed) 316L stainless steel parts by MAM. They reported that the polishability of the surface parallel to build direction was higher than the transverse surface. Munyensanga *et al.* [17] reviewed the application of MAM to polish AISI 316L stainless steel ball-bearing. They reported that a minimum Ra of 0.077 µm was achieved at optimal finishing conditions. Doshi and Vaghosi [18] finished aluminum alloy workpiece using Al_2O_3 based loosely bounded magnetic abrasives by MAM and reported that surface finish was enhanced by 29.9 to 71.21 %. Also, a significant value of Ra was reduced from 2.018 to 0.85 µm. Chaurasia and Wankhede [19] employed a MAM setup for finishing a flat workpiece of Inconel 718 superalloy using unbonded silicon carbide (SiC) based magnetic abrasives. They described that the most significant parameters were working gap and speed. Li *et al.* [20] processed titanium alloy wire by MAM. They reported that under the same processing time the surface finish was improved to 0.28 µm by MAM. Song *et al.* [21] proposed high-speed MAM to investigate the finishing characteristics of the ceramic bar. The minimum surface roughness Ra of 0.01 µm and roundness of 0.14 µm was achieved under optimum conditions. Ahmed *et al.* [22] proposed a statistical analysis to present the mathematical model of metal removal during the MAM process. The present study will shed light on the finishing of aluminum pipes in the magnetic abrasive machining tests. The objective of this research work is to use SiC-based glued magnetic abrasives in the internal finishing of aluminum pipes by MAM which was not attempted earlier.

The working principle of the magnetic abrasive machining (MAM) process involved in this paper is shown in **Figure 1**. The workpiece was placed between 2 magnets. With this configuration, magnetic abrasives could form an FMAB in the enforced magnetic field. As the workpiece rotates, a relative movement between the finishing brush and workpiece facilitated the mechanical material removal process. **Figure 1** shows the schematic diagram of the aluminum pipe finished by the MAM process. Under the influence of magnetic field strength, the magnetic abrasives were arranged along the direction of lines of the magnetic field and an FMAB with a specific finishing capacity was developed between the 2 magnetic poles. The developed FMAB wrapped the aluminum pipe internally. The FMAB is attracted by the magnetic pole to generate a relative motion with the aluminum pipe surface to be finished. The FMAB continuously cut and scratched the aluminum pipe surface wrapped inside. This micro removal of

material from the surface of the aluminum pipe results in the finishing of the surface and enhanced the quality of the surface.

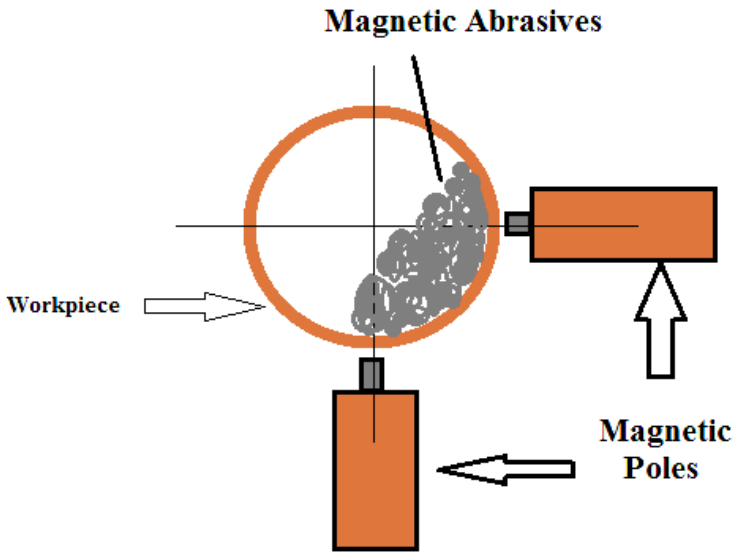

Figure 1 Schematic of internal magnetic abrasive machining (MAM).

Materials and methods

Experimental setup of magnetic abrasive machining (MAM)

Figure 2 illustrates a schematic of the experimental setup of MAM, which represents the principle of internal finishing. The major elements of MAM equipment include the electromagnet (12 k Gauss), variable DC supply, DC motor, control unit and magnetic abrasive powder (Glue-based SiC + Fe). The cylindrical workpiece viz. aluminum pipe was held in the chuck attached to the DC motor and magnetic abrasives were packed in the pipe. The magnetic field was applied to the magnetic abrasives by the electromagnet. Magnetic field strength (MFS) was changed for the experiments with the aid of variable DC supply. Electromagnet performs a prime role in present experimentation (2 cores of 40 mm diameter, core material-low carbon mild steel, number of turns-2500, and Copper wire gauge of 17 SWG). The space between workpiece and electromagnet is kept constant i.e. 1 mm. The magnitude of MFS depends on the weight percentage of magnetic particles, present in the magnetic abrasive powder. A DC motor was chosen to rotate the workpiece.

Experimental conditions

SiC-based glued magnetic abrasives were utilized for the internal finishing of cylindrical aluminum pipes (Ø36×Ø33×77 mm^3) in the current research work. These magnetic abrasives were prepared by mixing SiC (Silicon Carbide-400 mesh) abrasives and iron (ferromagnetic-300 mesh) powder. The mixture was thoroughly mixed after adding the Fevitite as glue. After proper setting of the mixture, it was crushed and sieved to different sizes. The obtained mesh sizes were varying from 60 - 250. Magnetic field strength (MFS), circumferential speed of workpiece, abrasive mesh size and quantity of abrasives were considered as input process parameters that would affect the surface roughness and material removal. PISF and MRR were taken as the response variables for the present study. PISF is calculated as (Initial Ra - Final Ra/Initial Ra)×100 and MRR is the ratio of reduction in weight of the workpiece and experiment time.

Four input parameters have been chosen, the values of parameters and their coded and actual levels were illustrated in **Table 1**. The preliminary experimentation was carried out to decide the levels of process parameters. The constant parameters along with their values are described in **Table 2**. After performing experiments, scanning electron microscopy (SEM) images were taken to compare the unfinished and finished workpieces.

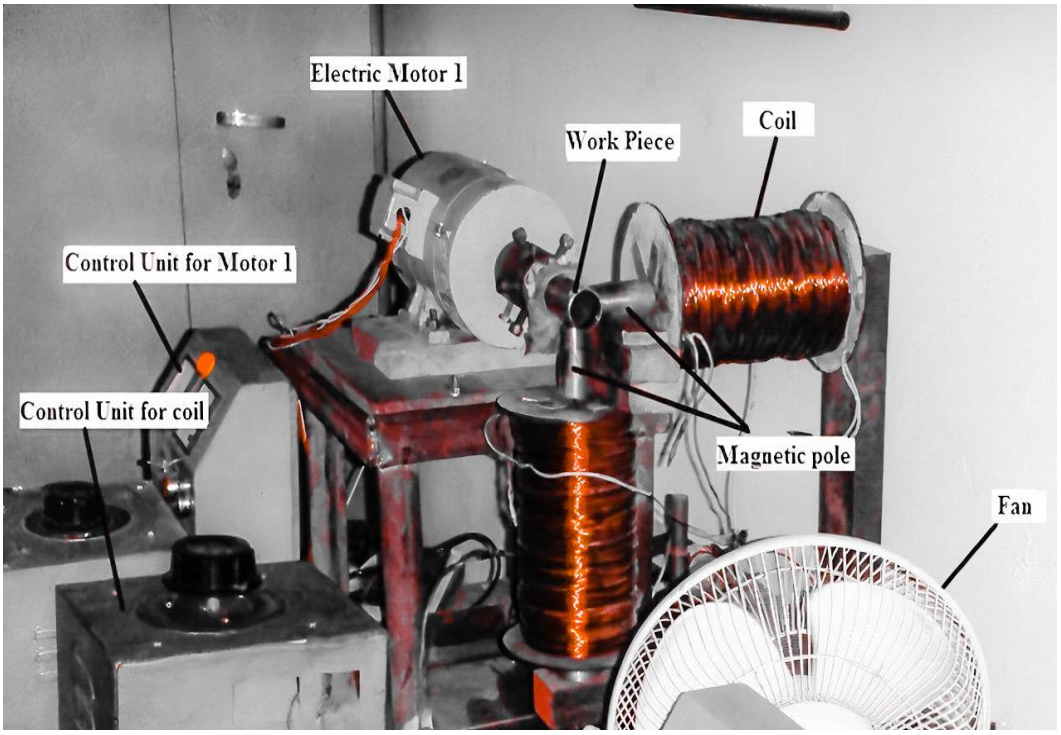

Figure 2 Photograph of experimental set up of MAM.

Table 1 Levels and description of process parameters.

Coded	Description	Abbreviation	Level				
			−2	**−1**	**0**	**1**	**2**
A	Magnetic field strength (Gauss)	MFS	7,000	8,000	9,000	10,000	11,000
B	Circumferential speed of workpiece (rpm)	Speed	600	800	1,000	1,200	1,400
C	Abrasive mesh size	Mesh size	60	80	120	160	250
D	Quantity of abrasives (g)	Quantity	5	10	15	20	25

Table 2 Constant process parameters.

Parameter	Lubricant	Pole vibration	Workpiece-pole gap	Experiment time
Description/value	Kerosene oil (5 % of the quantity of abrasives)	Amplitude: 5 mm; frequency: 0.8 Hz	1 mm	30 min

Model fitting and statistical examination

Central composite design (CCD) was employed in this work involving four input variables. The design of experiments and statistical examination was performed with the aid of Design-Expert software. Moreover, this software has also been utilized for the regression analysis of experimental data, to plot various graphs and contour plots. The adequacies of the models were checked with respect to adjusted values. The analysis of variance (ANOVA) was utilized to find out the significance of models. The optimization of process conditions and predicted values were performed to confirm the validation of

models. In a statistical examination, the modeling of the responses along with process parameters was done to optimize the process conditions for the required responses. The ANOVA was utilized for the calculation of the statistical parameters. The statistical significance was checked by the F-test.

Results and discussion

The input parameters were applied according to the design matrix generated by central composite design (CCD) of response surface methodology (RSM) and the output/responses (PISF & MRR) were shown in **Table 3**. Surface finish before and after finishing was measured using a Mitutoyo surface roughness tester having LC = 0.001 µm and weight was noted using precision electronic balance having LC = 0.1 mg. The maximum PISF of 81.5 % and the corresponding minimum Ra value of 0.07 µm were achieved. The statistical data was acquired for the finishing of aluminum pipes using MAM. The effects of interactions of different process parameters such as magnetic field strength (MFS), circumferential speed, mesh size and quantity on PISF and MRR were examined utilizing RSM. Further, optimization of parameters on PISF and MRR are represented.

Statistical analysis for selected models

The analysis of variance (ANOVA) was performed at 95 % confidence level for PISF and MRR. ANOVA of suggested models showed that both models were highly significant, evident from Fisher's F-test with high F value and low *p*-value. The lack of fit (LOF) was not significant for both the models which is good to fit the models. There is reasonable agreement between predicted R^2 and adjusted R^2 because of the negligible difference for both the suggested quadratic models. So, developed models are acceptable for both PISF and MRR. The adjusted R^2 values for PISF and MRR were 0.9875 and 0.9973, respectively, which are also high and specify a high correlation between the experimental and predicted values.

The complete ANOVA outcomes for PISF and MRR are tabulated in **Table 4**. It was observed that the outcomes between the predicted and experimental were in near agreement for both PISF and MRR. The predicted and experimental values of both the responses are following the fitted line as described in **Figures 3** and **4**, respectively. This indicates that the model is appropriate and can be utilized straight on the shop floor. The developed models for PISF and MRR are significant. The adequacy precision viz. signal to noise ratio (S/N) is more than 4 for both the models which show the adequacy of the models.

Table 3 Central composite design arrangement and responses.

Exp. No.	A: MFS (Gauss)	B: Speed (rpm)	C: Mesh size	D: Quantity (g)	PISF (%)	MRR (mg/min)
1	10,000	1,200	80	20	71.2	2.3
2	9,000	1,000	250	15	61.1	1.9
3	9,000	1,000	120	15	75.9	2.07
4	8,000	1,200	160	20	40.1	0.96
5	10,000	800	80	20	62.8	1.83
6	8,000	800	80	10	60.5	1.66
7	8,000	1,200	160	10	46.2	1.04
8	8,000	1,200	80	20	45.6	1.32
9	10,000	1,200	80	10	**81.5**	**2.70**
10	9,000	1,000	60	15	66.1	2.46
11	9,000	1,000	120	15	75.9	2.07
12	9,000	600	120	15	65.1	1.47
13	10,000	800	80	10	72.2	2.01
14	8,000	1,200	80	10	51.2	1.58
15	9,000	1,000	120	15	74.4	2.04
16	11,000	1,000	120	15	63.1	2.60
17	7,000	1,000	120	15	27.6	1.38
18	8,000	800	80	20	51.6	1.5

Exp. No.	A: MFS (Gauss)	B: Speed (rpm)	C: Mesh size	D: Quantity (g)	PISF (%)	MRR (mg/min)
19	9,000	1,000	120	15	73.6	2.04
20	10,000	800	160	10	70.8	1.78
21	8,000	800	160	20	51.4	1.47
22	10,000	1,200	160	10	70.2	2.0
23	10,000	1,200	160	20	64.4	1.87
24	10,000	800	160	20	60.8	1.78
25	8,000	800	160	10	60.8	1.5
26	9,000	1,000	120	15	73.8	2.08
27	9,000	1,400	120	15	60.9	1.58
28	9,000	1,000	120	5	65.4	1.25
29	9,000	1,000	120	15	72.7	2.06
30	9,000	1,000	120	25	52.4	0.97

Table 4 ANOVA for experimental data.

Source	SSque	DF	MSque	F Value	*p*-value Prob > F	Remarks
Percentage Improvement in Surface Finish (PISF)						
Model	4,364.43	14	311.74	164.01	< 0.0001	SGFT
A: MFS	1,971.09	1	1,971.09	1,037.02	< 0.0001	SGFT
B: Speed	34.80	1	34.80	18.31	0.0007	SGFT
C: Mesh size	60.18	1	60.18	31.66	< 0.0001	SGFT
D: Quantity	348.84	1	348.84	183.53	< 0.0001	SGFT
AB	239.48	1	239.48	125.99	< 0.0001	SGFT
AC	7.70	1	7.70	4.05	0.0624	Non-SGFT
AD	1.89	1	1.89	0.9947	0.3344	Non-SGFT
BC	40.01	1	40.01	21.05	0.0004	SGFT
BD	6.13	1	6.13	3.22	0.0928	Non-SGFT
CD	0.5256	1	0.5256	0.2765	0.6067	Non SGFT
A^2	1,372.91	1	1,372.91	722.31	< 0.0001	SGFT
B^2	197.06	1	197.06	103.68	< 0.0001	SGFT
C^2	37.77	1	37.77	19.87	0.0005	SGFT
D^2	375.74	1	375.74	197.68	< 0.0001	SGFT
Residual	28.51	15	1.90			
LOF	20.12	10	2.01	1.20	0.4456	Non-SGFT
Adjusted R^2 = 0.9875, **Predicted R^2** = 0.9736, **Adeq Precision** = 53.07						
Material Removal Rate (MRR)						
Model	5.73	14	0.4096	766.32	< 0.0001	SGFT
A: MFS	2.52	1	2.52	4718.35	< 0.0001	SGFT
B: Speed	0.0054	1	0.0054	10.10	0.0062	SGFT
C: Mesh size	0.4806	1	0.4806	899.19	< 0.0001	SGFT
D: Quantity	0.1204	1	0.1204	225.28	< 0.0001	SGFT
AB	0.4225	1	0.4225	790.44	< 0.0001	SGFT

Source	SSque	DF	MSque	F Value	*p*-value Prob > F	Remarks
AC	0.0030	1	0.0030	5.66	0.0311	SGFT
AD	0.0004	1	0.0004	0.7483	0.4006	Non-SGFT
BC	0.1332	1	0.1332	249.25	< 0.0001	SGFT
BD	0.0100	1	0.0100	18.71	0.0006	SGFT
CD	0.0272	1	0.0272	50.93	< 0.0001	SGFT
A^2	0.0021	1	0.0021	3.88	0.0675	Non-SGFT
B^2	0.5142	1	0.5142	962.07	< 0.0001	SGFT
C^2	0.0707	1	0.0707	132.25	< 0.0001	SGFT
D^2	1.58	1	1.58	2961.94	< 0.0001	SGFT
Residual	0.0080	15	0.0005			
LOF	0.0066	10	0.0007	2.36	0.1774	Non-SGFT

Adjusted R^2 = 0.9973, **Predicted R^2** = 0.9939, **Adeq Precision** = 105.28

SSque - Sum of Squares; DF-Degree of freedom; MSque- Mean Square; LOF-Lack of Fit; SGFT-Significant

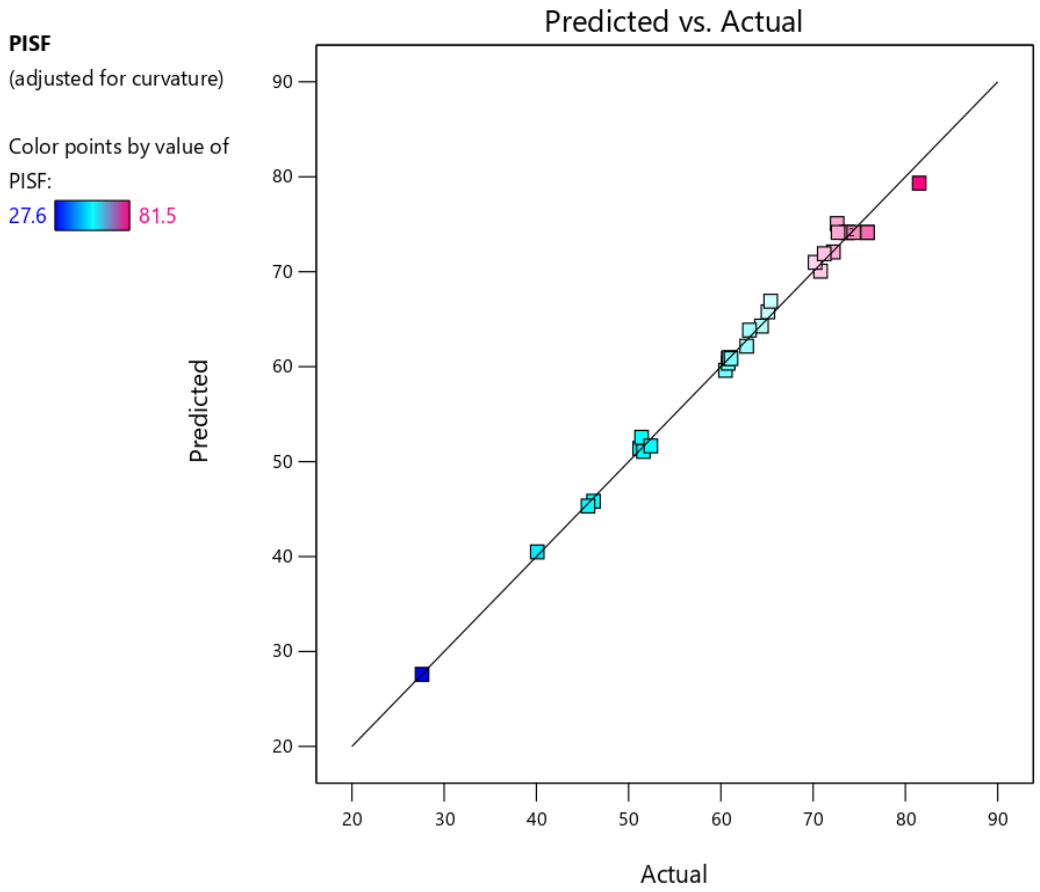

Figure 3 Predicted vs actual plot for PISF.

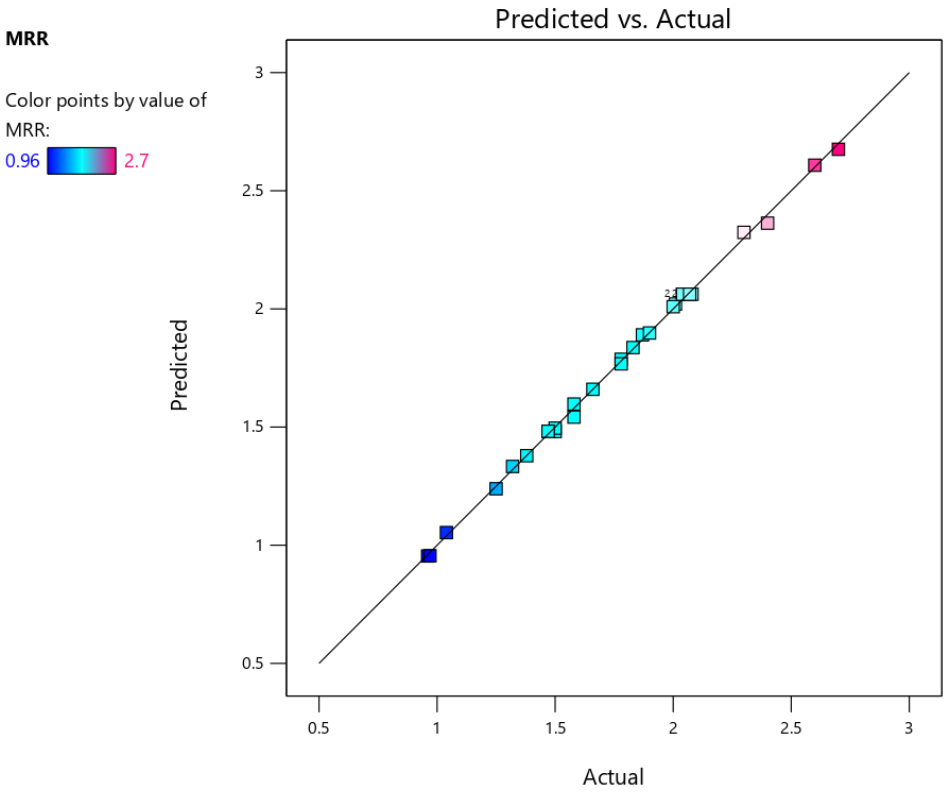

Figure 4 Predicted vs actual plot for MRR.

Development of the models

The regression analysis of the experimental data has been investigated and 3D interaction plots have been drawn by using statistical Design-Expert software. The quadratic models of both the responses (PISF and MRR) with respect to actual parameters are given beneath:

$$PISF = -534.266 + 0.120701 \times MFS - 0.0311096 \times Speed + 0.406847 \times Mesh\ Size + 3.5883 \times Quantity + 1.93437e\text{-}05 \times MFS \times Speed - 1.73438e\text{-}05 \times MFS \times Mesh\ Size - 6.875e\text{-}05 \times MFS \times Quantity - 0.000197656 \times Speed \times Mesh\ Size + 0.00061875 \times Speed \times Quantity + 0.00090625 \times Mesh\ Size \times Quantity - 7.10385e\text{-}05 \times MFS^2 - 6.72837e\text{-}05 \times Speed^2 - 0.000456348 \times (Mesh\ Size)^2 - 0.148654 \times Quantity^2$$

$$MRR = -0.856118 - 0.000274858 \times MFS + 0.00138049 \times Speed + 0.00283992 \times Mesh\ Size + 0.28456 \times Quantity + 8.125e\text{-}07 \times MFS \times Speed - 3.4375e\text{-}07 \times MFS \times Mesh\ Size - 1e\text{-}06 \times MFS \times Quantity - 1.14062e\text{-}05 \times Speed \times Mesh\ Size - 2.5e\text{-}05 \times Speed \times Quantity + 0.00020625 \times Mesh\ Size \times Quantity - 8.73475e\text{-}09 \times MFS^2 - 3.43712e\text{-}06 \times Speed^2 + 1.97434e\text{-}05 \times (Mesh\ Size)^2 - 0.00964939 \times Quantity^2$$

Influence of input process parameters on the PISF and MRR

The process parameter has a significant impact on the PISF and MRR, the output parameters of the MAM process, (**Table 3**), and as well as the mechanism of the process. There are 2 types of forces present, causing the capability of surface finishing of the specimen and these forces are generated by FMAB. These normal forces provide the packaging of magnetic abrasives and causing the micro-indentations into the specimen while the tangential cutting forces lapping the specimen due to the rotation effect of the abrasive material mixture (iron particles) and resulting in the removal of surface material on the aluminum pipe. The good finish and accuracy of surface finish with minimum defects or burrs is cost-effective by MAM than machining with conventional methods such as grinding and

polishing. This gives to the manufacturer to integrate the new technology of advanced machining with non-conventional techniques including MAM upon the ability to generate: (1) a very high surface finish and accuracy. (2) very little or no surface damage.

***Influence of interactions between magnetic field strength (A) & speed (B) on* PISF**

Figure 5 illustrates the influence of the combined variation of MFS & speed on PISF. It can be seen from the plot that at low values of speed, PISF first increases then start to stabilize with the increase in values of MFS, whereas at high values of speed, PISF goes on increasing with an increase in MFS. When MFS increased, PISF increased due to higher MFS in a specified gap. The increased MFS leads to an increase in strength and area of contact of the FMAB. Higher-strength of field causes more force on the abrasive tool and increases the finishing force. This increase can lead to finer surface roughness. It is not possible to obtain a good surface finish at lower values of MFS & speed. PISF is best at higher values of MFS & speed, due to more forces acting on the abrasives. Djavanroodi [23] reported that at low MFS, PISF was low but, as the MFS increased and FMAB toughness also increased (a higher force for holding particles in the direction of field), which resulted in increased PISF.

***Influence of interactions between speed (B) & mesh size (C) on* PISF**

Figure 6 shows the influence of simultaneous variation of speed & mesh size on PISF. It can be seen that by increasing the speed at higher mesh size, PISF first starts increasing slowly, and with the further increase in speed, PISF decreased more rapidly. This is because of the reason that increased rotational speed has increased the centrifugal force acting on the abrasive grains which cause ejection of grains from the finishing surface. It is evident from **Figure 6** that at the same level of speed, mid and higher mesh size (small particle size) of abrasives leads to more improvement in surface finish. This is due to the fact that with increased mesh size, the number of abrasive particles per unit volume increased, and because of which the number of cutting edge per unit area increased which resulted in the increased PISF [24]. Another reason for this may be that with the increased mesh size, the abrasives form a very fine cutting edge thereby improving the surface finish, however when the particle size is further decreased the iron and abrasive components tend to separate thereby causing a negligible increase in PISF. The value of PISF is least at maximum values of both speed & mesh size because fine particles are carried away at high speed. Better PISF can be acquired at high speed and lower values of mesh size of the abrasive particles.

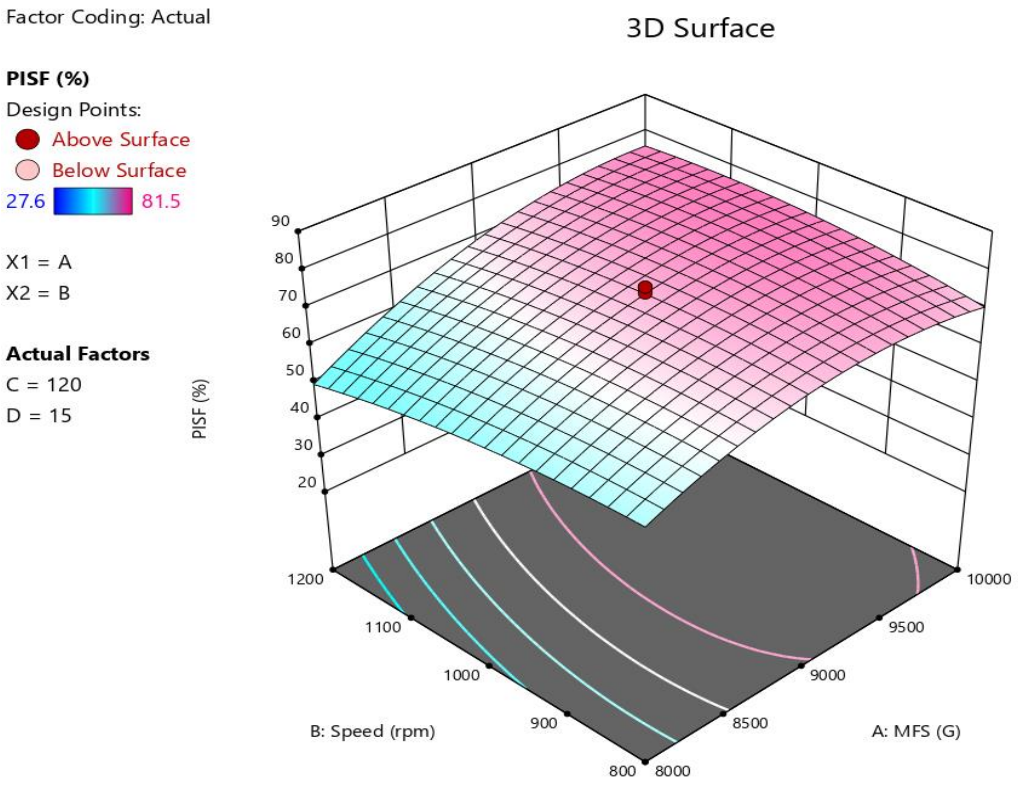

Figure 5 Influence of interactions between Magnetic Field Strength (MFS) & speed on PISF.

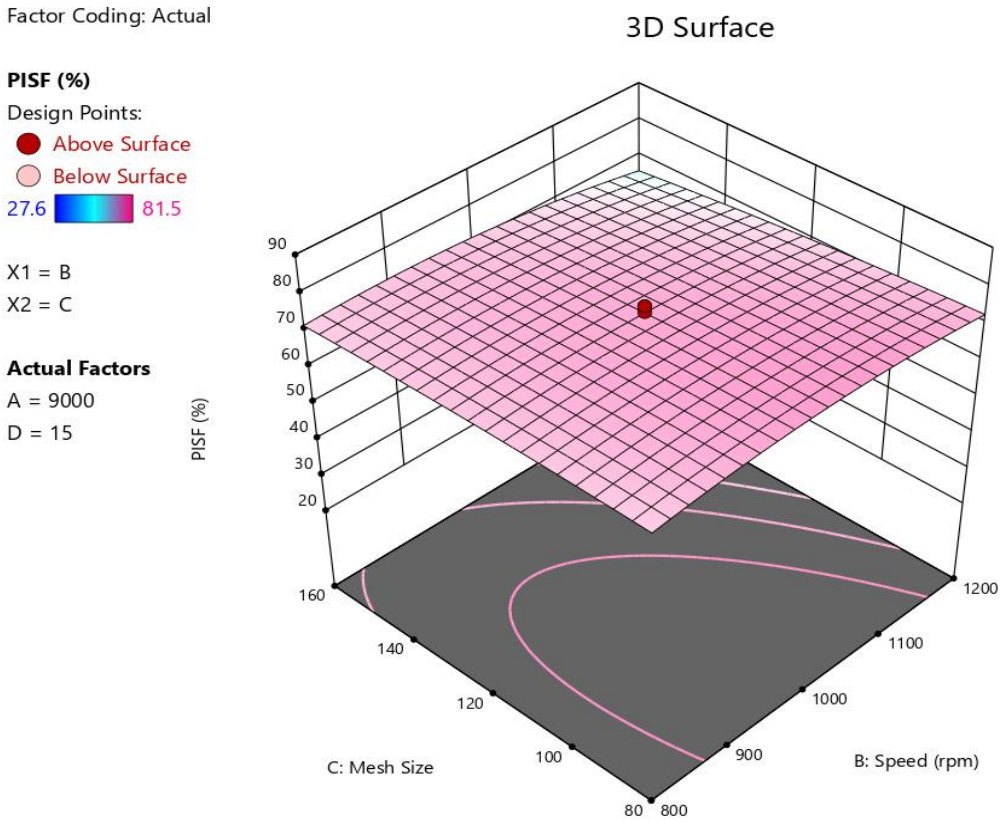

Figure 6 Influence of interactions between speed & mesh size on PISF.

***Influence of interactions between MFS (A) & mesh size (C) on* PISF**

Figure 7 shows the influence of simultaneous variation of MFS & mesh Size on PISF. It can be seen that at all levels of mesh size, with increased MFS, PISF goes on increasing. The increased MFS leads to increased strength and area of contact of the FMAB. The higher strength of field causes more force on the abrasive tool and increases the finishing force. This increase can lead to a finer surface finish. It can also be seen from **Figure 7**, at all levels of MFS with increased mesh size, there is negligible improvement in surface finish. This may be due to the reason that with the increased mesh size, the abrasives form a very fine cutting edge thereby improving the surface finish, however when the particle size is further decreased the iron and abrasive components tend to separate thereby causing a negligible increase in PISF.

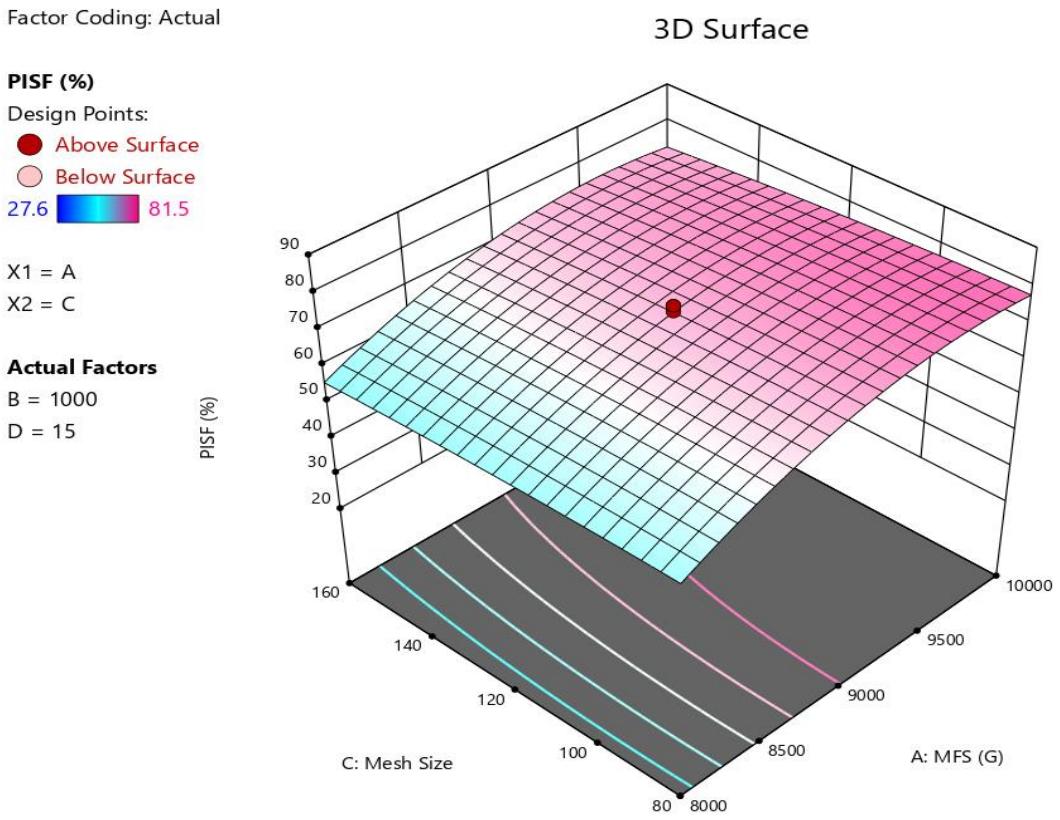

Figure 7 Influence of interactions between Magnetic Field Strength (MFS) & mesh size on PISF.

***Influence of interactions between magnetic field strength (A) & speed (B) on* MRR**

The 3D plot shows the influence of simultaneous variation of MFS and speed on MRR (**Figure 8**). With the increased MFS at all values of rotational speed, there is a continuous increase in the value of MRR, on the other hand at a higher value of MFS, with the increased rotational speed, MRR goes on increasing. This is due to the reason that the effect of getting the highest magnitude of magnetic force causes the change in the increased value of the packing density of the magnetic abrasive particles used. Consequently, the rigidity of the flexible magnetic abrasive particles changes also their magnetic force by becoming larger and resulting in deeper micro indentations into the specimen, thus increasing the MRR. But the value of MRR acquired is greater at mid-value of speed and high MFS than obtained at low speed & low MFS. As per literature, MRR increased with the workpiece rotational speed and after some value of speed, jumbling of magnetic abrasives started which decreased the value of MRR. **Figure 8** also shows that at the low value of MFS, PISF increases up to 1,100 rpm and then starts decreasing.

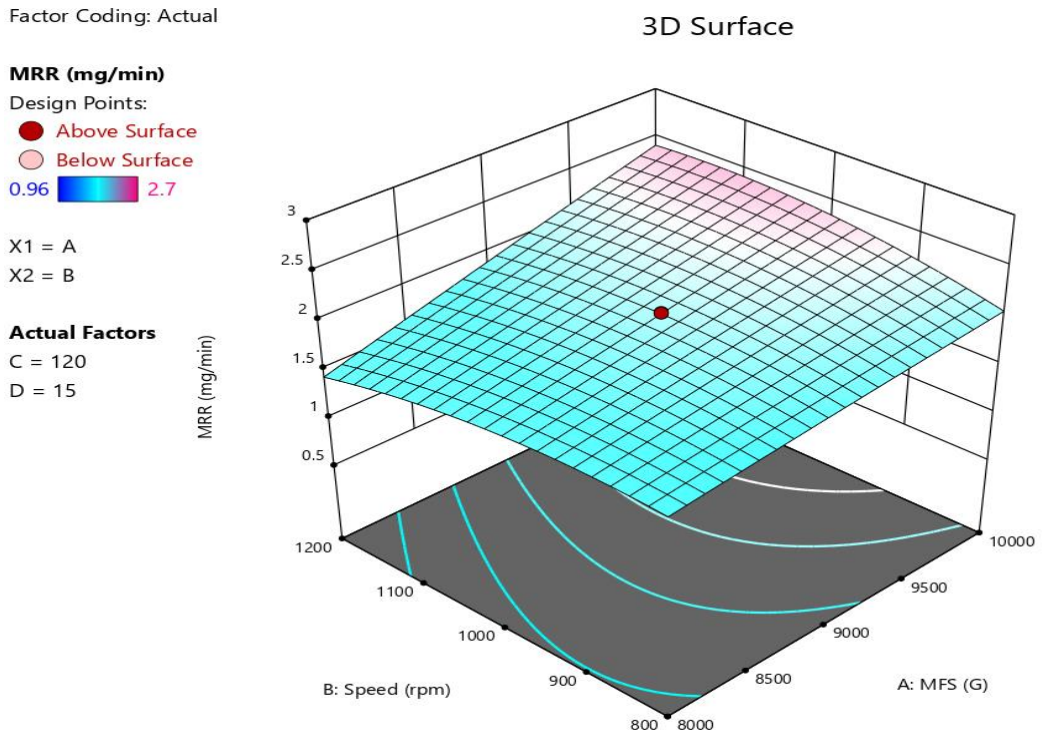

Figure 8 Influence of interactions between magnetic field strength & speed on MRR.

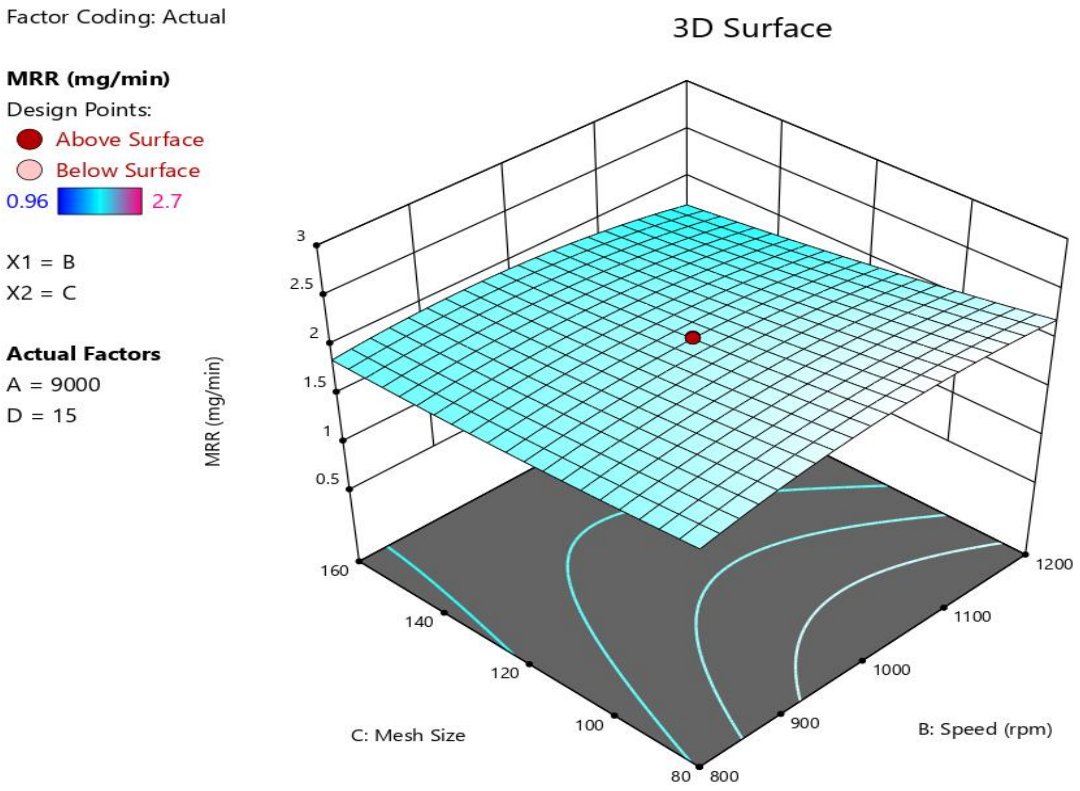

Figure 9 Influence of interactions between speed & mesh size on MRR.

***Influence of interactions between speed (B) & mesh size (C) on* MRR**

The 3D plot illustrates the influence of the interaction of speed and mesh size on MRR (**Figure 9**). At low speed, MRR almost remains constant with the increased mesh size and at high speed, MRR goes on decreasing with the increased mesh size. This is because, with the increased mesh number, the number of abrasive particles per unit volume becomes very high and these particles get inserted between 2 iron particles [25]. As a result, the shearing strength of magnetic abrasive brush decreased which resulted in a decreased value of MRR. It can be seen that the value of MRR comes down more exceptionally at the high value of speed and mesh size of the abrasives because high speed leads to jumbling of the magnetic abrasive particles. This is due to the fact that with the increased rotational speed, the centrifugal force also increased, and at a very high value of speed, this force tends to fly the abrasives from the magnetic field which resulted in a small MRR.

***Influence of interactions between MFS (A) & mesh size (C) on* MRR**

The 3D plot shows the influence of simultaneous variation of MFS and mesh size on MRR (**Figure 10**). With the increased MFS at all values of mesh size, there is a continuous increase in the value of MRR. This is due to the reason that the rigidity of the FMAB changes also its magnetic force by becoming larger and resulting in deeper micro indentations into the specimen, thus increasing the MRR. On the other hand, at a higher value of MFS, with the increased mesh size, MRR goes on decreasing. This is because, with the increased mesh number, the number of abrasive particles per unit volume becomes very high and these particles get inserted between 2 iron particles [25]. As a result, the shearing strength of the magnetic abrasive brush decreased which resulted in a decreased value of MRR.

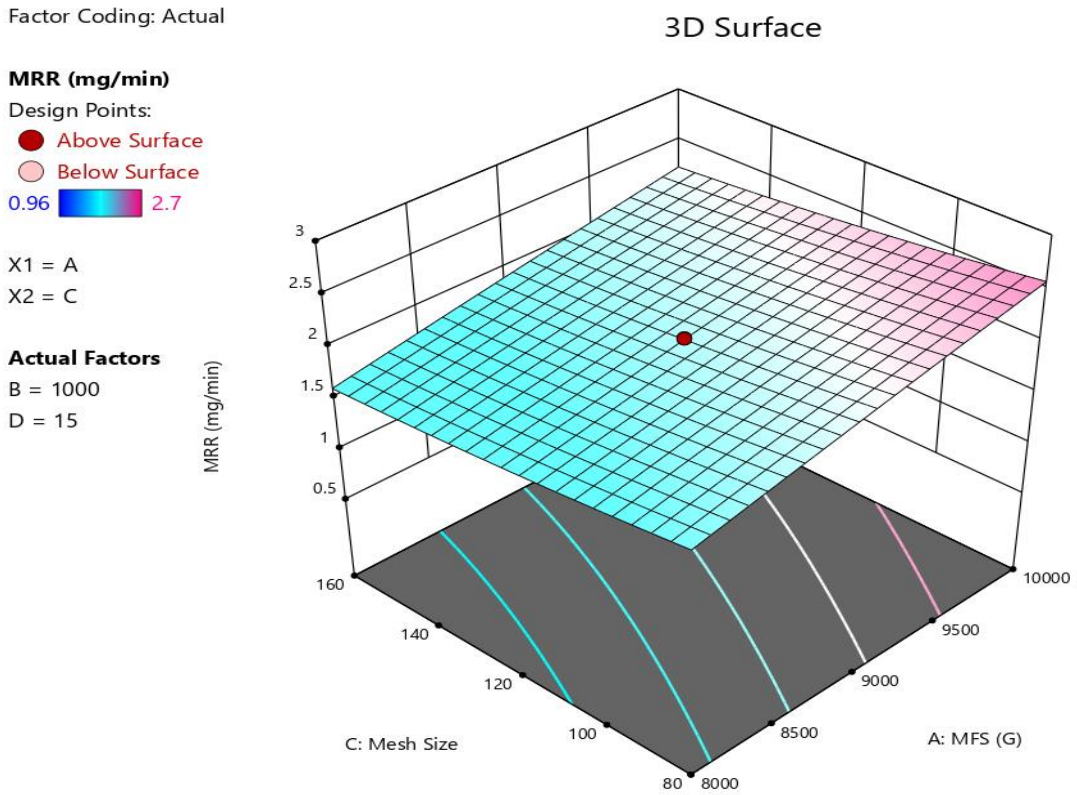

Figure 10 Influence of interactions between Magnetic Field Strength (MFS) & mesh size on MRR.

Optimization of process parameters

For identifying the combination of process parameters that results in maximum PISF and MRR, developed models for the PISF & MRR were optimized. The values of process parameters at which the models were optimized are given in **Table 5**. The experiments were performed in triplet at the optimized parameters to check the accuracy and precision of the developed models.

Table 5 Comparison of PISF and MRR at optimum parameters.

Exp. No.	MFS (Gauss)	Speed (r,pm)	Mesh size	Quantity (g)	Pred. PISF (%)	Exp. PISF (%)	Pred. MRR (mg/min)	Exp. MRR (mg/min)
1	10,000	1,200	80	10	81.7	81.6	2.60	2.63
2	10,000	1,200	80	10	81.6	81.4	2.64	2.65
3	10,000	1,200	80	10	81.3	81.2	2.61	2.58

Surface conditions

Reflection method examination

Figure 11 illustrates the surface conditions before and after finishing when process parameters are preset, 10,000 Gauss of magnetic field strength (MFS), 1,200 rpm of circumferential speed of workpiece, 80 abrasive mesh size and 10 g of the quantity of abrasives and there is the unfinished surface condition of the aluminum pipe with a very poor degree of reflection being not readable for the letter A at the bottom side of the aluminum pipe. Whereas, the finished surface condition applied by MAM for 30 min has a good degree of reflection that is sufficient to easily read the letter B & C. The value of the surface finish was improved by more than 80 %.

Figure 11 A view of the surface finish obtained in one of the samples after MAM.

SEM analysis

SEM micrographs of the workpiece surface before and after the magnetic abrasive machining (MAM) are shown in **Figures 12(a) - 12(b)**, respectively. Surface roughness (Ra) and material removal during finishing for aluminum pipe are presented in **Figure 12(b)**. It is noted that though the unfinished sample had a rougher initial surface than the finished sample, its surface roughness Ra was improved more rapidly from ~0.38 to 0.07 μm (Ra) after a 30 min finishing. It could be seen that the peaks of the initial surface were removed while the valleys were still retained. The observations reveal that the grinding marks were almost removed by magnetic abrasive machining (MAM). Therefore, it can be seen that MAM is capable of finishing aluminum pipes.

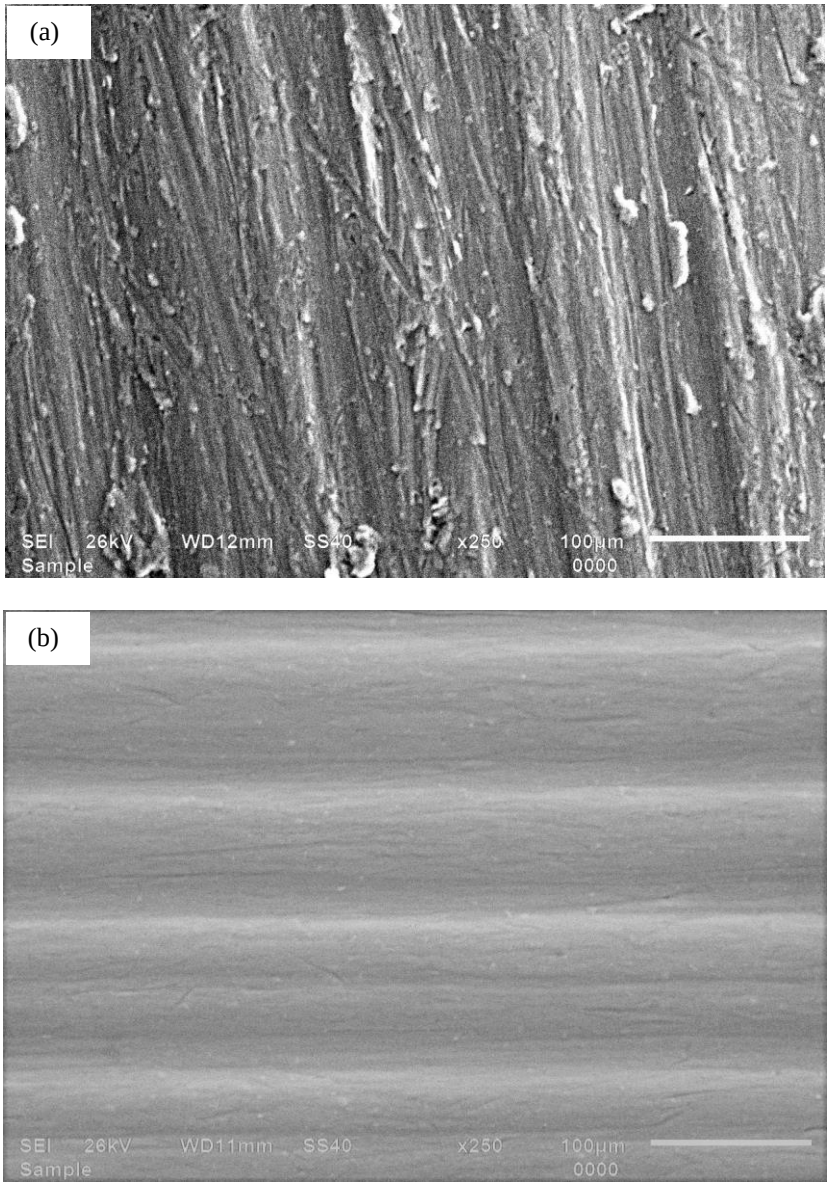

Figure 12 SEM graphs of inner surface of aluminum pipe: (a) before finishing and (b) after finishing for 30 min.

Conclusions

The magnetic abrasive machining (MAM) process for the finishing of aluminum pipes with the use of SiC-based glued magnetic abrasives (SiC 400 mesh and Fe 300 mesh) has been carried out in this work. As per the ANOVA table, magnetic field strength (MFS), abrasive mesh size and quantity of abrasives are the parameters that significantly influence percentage improvement in surface finish (PISF), and material removal rate (MRR) and circumferential speed of workpiece is the least significant parameter. The interactions between MFS and speed have the highest significant effect on both PISF and MRR. The value of surface roughness was decreased and PISF was almost 27.6 - 81.5 %. The optimum value of process parameters viz. magnetic field strength (MFS), circumferential speed of workpiece, abrasive mesh size and quantity of abrasives is 10000 G, 1200 rpm, 80 and 10 g, respectively for the maximum value of PISF = 81.5 % and corresponding maximum surface finish (Ra) 0.07 µm was acquired. SEM of workpieces before and after magnetic abrasive machining shows that the surface finish improves after magnetic abrasive machining.

Acknowledgements

The authors express heartfelt thanks to Baba Banda Singh Bahadur Engineering College, Fatehgarh Sahib, India for their continuous support.

References

[1] F Hashimoto, H Yamaguchi, P Krajnik, K Wegener, R Chaudhari, HW Hoffmeister and F Kuster. Abrasive fine-finishing technology. *CIRP Ann.* 2016; **65**, 597-620.
[2] H Yamaguchi and T Sato. *Polishing and magnetic field-assisted finishing. In*: W Zhang (Ed.). Intelligent energy field manufacturing interdisciplinary process innovations. CRC Press, Florida, USA, 2012.
[3] DK Singh, VK Jain and V Raghuram. Superfinishing of alloy steels using magnetic abrasive finishing process. *In*: Proceedings of the18th Annual ASPE Meeting, Portland, USA. 2003, p. 5-8.
[4] P Singh, PS Samra and L Singh. Internal finishing of cylindrical pipes using sintered magnetic abrasives. *Int. J. Eng. Sci. Tech.* 2011; **3**, 5747-53.
[5] P Singh and L Singh. *Optimization of magnetic abrasive finishing parameters with response surface methodology. In*: S Khangura, P Singh, H Singhand and G Brar (Eds.). Proceedings of the International Conference on Research and Innovations in Mechanical Engineering. Lecture Notes in Mechanical Engineering. Springer, New Delhi, India, 2014, p. 273-86.
[6] S Singh and L Singh. Effect of magnetic abrasives in internal finishing of brass tubes using MAF method. *J. Acad. Ind. Res.* 2014; **2**, 689-92.
[7] MG Patil, K Chandra and PS Misra. Study of mechanically alloyed magnetic abrasives in magnetic abrasive finishing. *Int. J. Sci. Eng. Res.* 2012; **3**, 532-6.
[8] PS Kang, L Singh and JS Gill. Finishing of SUS 304 stainless steel bent tubes using magnetic abrasive finishing. *Mechanica. Confab. Int. J.* 2013; **2**, 123-30.
[9] A Kaushik, P Singh and L Singh. *Finishing of aluminum pipes using silica sand (river bed)-based loosely bonded magnetic abrasives. In*: S Khangura, P Singh, H Singhand and G Brar (Eds.). Proceedings of the International Conference on Research and Innovations in Mechanical Engineering. Lecture Notes in Mechanical Engineering. Springer, New Delhi, India, 2014, p. 297-303.
[10] HS Grewal, A Singh and J Singh. Effect of various parameters on finishing of inner surfaces of brass tubes using magnetic abrasive by RSM: A study. *Asian Rev. Mech. Eng.* 2015; **4**, 43-52.
[11] AY Jiao, HJ Quan, ZZ Li and Y Chen. Study of magnetic abrasive finishing in seal ring groove surface operations. *Int. J. Adv. Manuf. Tech.* 2016; **85**, 1195-205.
[12] N Sihag, P Kala and PM Pandey. Analysis of surface finish improvement during ultrasonic assisted magnetic abrasive finishing on chemically treated tungsten substrate. *Procedia Manuf.* 2017; **10**, 136-46.
[13] H Yamaguchi, O Fergani and PY Wu. Modification using magnetic field-assisted finishing of the surface roughness and residual stress of additively manufactured components. *CIRP Ann.* 2017; **66**, 305-8.
[14] GC Verma, P Kala and PM Pandey. Experimental investigations into internal magnetic abrasive finishing of pipes. *Int. J. Adv. Manuf. Tech.* 2017; **88**, 1657-68.
[15] Deepak and B Bhusan. Experimental analysis of improvement of surface finishing using magnetic abrasive finishing. *Int. J. Tech. Res.* 2017; **6**, 1-7.
[16] J Zhang, WG Tai, G Wang, SK Anantharajan, WF Lu and JYH Fuh. Magnetic abrasive polishing of additively manufactured 316L stainless steel parts. *In*: Proceedings of the EUSPEN's 18th International Conference & Exhibition, Venice, Italy. 2018, p. 401-2.
[17] P Munyensanga, P Paryanto and MNA Aziz. Application of polishing AISI 316L stainless steel ball bearing with a magnetic abrasive finishing process: A review. *Rotasi* 2019; **20**, 249-57.
[18] SJ Doshi and KS Vaghosi. Some investigations on magnetic abrasive finishing of aluminium alloy. *Int. J. Res. Anal. Rev.* 2018; **5**, 401-6.
[19] A Chaurasia and V Wankhede. Magnetic abrasive finishing of inconel 718 super alloy using permanent magnet. *Int. Res. J. Eng. Tech.* 2018; **5**, 1165-8.
[20] W Li, Y Chen, M Cheng and Y Lv. Effect of magnetic head shape on processing of titanium alloy wire by magnetic abrasive finishing. *Materials* 2020; **13**, 1401.
[21] J Song, T Shinmura, SD Mun and M Sun. Micro-machining characteristics in high-speed magnetic abrasive finishing for fine ceramic bar. *Metals* 2020; **10**, 464.
[22] BA Ahmed, SK Shather and WK Hamdan. Statistical analysis of metal removal during magnetic

abrasive finishing process. *J. Eng*. 2020; **26**, 34-45.
[23] F Djavanroodi. Artificial neural network modeling of surface roughness in magnetic abrasive finishing process. *Res. J. Appl. Sci. Eng. Tech.* 2013; **6**, 1976-83.
[24] P Kala and PM Pandey. Comparison of finishing characteristics of two paramagnetic materials using double disc magnetic abrasive finishing. *J. Manuf. Process.* 2015; **17**, 63-77.
[25] RS Mulik and PM Pandey. Ultrasonic assisted magnetic abrasive finishing of hardened AISI 52100 steel using unbonded SiC abrasives. *Int. J. Refract. Met. Hard Mater.* 2011; **29**, 68-77.